

3D FE model reconstruction and numerical simulation of airflow for the upper airway

Yingxi Liu¹, Chi Yu^{1*}, Xiuzhen Sun², Jizhe Wang²

¹ State Key Lab. of Strict. Anal. for Ind. Equip., Dalian Univ. of Technol., Dalian 116024, China

² Department of Otorhinalaryngology, the Second Affiliated Hospital of Dalian Medical University, Dalian 116023, China

(Received November 18 2005, accepted January 03 2006)

Abstract. Based on CT medical images of ten volunteers, the 3D FE model of the upper airway was reconstructed by using the method of surface rendering. It is comparatively true that the established model reflects the actual anatomical configuration, and the airflow of the whole cavity is simulated numerically and analyzed by the FE method. From the results of the numerical simulation, the airflow distribution in the whole cavity and pharyngeal cavities in the course of respiration can be obtained. The results of the numerical simulation can be used to diagnose the disease related to the anatomical structure and the function of the upper airway and the additional study of the pathogenesis.

Keywords: upper airway, pharyngeal cavity, three-dimensional finite element reconstruction, computational fluid dynamics numerical model

1 Introduction

The upper airway of a human is the main thoroughfare for eupnoea. In recent years, as a result of the study of pathogenesis of nasosinusitis and the SAS (Sleep Apnea Syndrome), people think that some diseases of the upper airway are related to the structure of the upper airway. In recent years, advances in the biological and medical sciences have increasingly relied on modeling and simulation^[8]. Previous efforts had been made to model the upper airway of adults as in vitro casts in order to determine airflow characteristics in this region. Ravi P. Subramaniam et al^[10], using the finite element method, developed a computational model of a nasal cavity and conducted numerical simulation under steady state. The information used in the reconstruction came from magnetic resonance imaging scans of the nose of a healthy male. Alipour et al^[11], studied an excised canine larynx, a Plexiglas reconstruction, and a computational model. Parabolic laminar velocity profiles were noted prior to the glottis restriction and were followed by an asymmetric turbulent jet (the laryngeal jet) in all models. Other simulations when combined with computational^[6] and experimental studies have shown similar results^[3].

Recent computational models of fluid flow in the adult upper airways have been presented for a smoothed model^[5] that identified similar patterns as the work of Corcoran and Chigier^[2]. This model extended from the mouth through the trachea utilized a modified low Reynolds number (LRN) $k - \omega$ turbulence model, addressing the unsuitability of the $k - \varepsilon$ model to predict particle deposition^[9]. S. K. Kim^[7] replicated a resin prototype of a normal nasal cavity from computer files to study airflow in a normal and abnormal nasal cavity. But the multi- examples, of three dimensional finite element reconstruction concerning the nose, pharynx, and throat structure, has not been reported. In this paper, the 3D FE models of the upper airway were constructed.

* Corresponding author. Tel.: +86-411-84708403; fax: +86-411-84708403.
E-mail address: yuchiyuchi@163.com.

The data was obtained from 10 healthy people. The numerical simulations and analysis for the flow in those pharyngeal cavities were completed.

2 Methods

2.1 Model generation

The volunteers were 10 adults, 4 males and 6 females, with no disease history of the upper respiratory tract. Their avoirdupois index was normal.

The data for reconstruction came from CT scans which provided coronal CT images of the volunteers. The reconstruction of the upper airway cavity was conducted by the method of surface rendering. The CT images (Fig. 1) include three colors of black, white and gray.

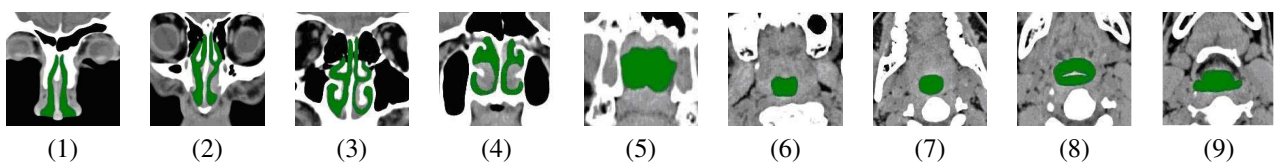


Fig. 1. Selected ct images

The density of the cavum is the lowest, thus, is black in the image. The bone tissues have the highest density and are white in the image. The soft tissues are of different density and are seen as a gray color. The CT images are made digitally by the Matlab software. According to the image resolution, the software can convert the CT image into a matrix in which every number factor corresponds to the value of the gray-scale of the pels. Some programs are made to determine the boundary of the wall in the nasal cavity. This characteristic is used to help judge the boundary. The black pels which represent the cavum correspond to the value of zero. The information of boundary points can be acquired after all the images are converted. With the information loaded into the Ansys software, the points can be plotted. With the entire boundary points being connected, the reconstruction of the upper airway cavity volume is completed. Then, the 1:1 reconstruction model can be obtained, based on the proper scale. Based on the pels, the upper airway wall would be reproduced accurately. Fig. 2 shows the particular region of the airway which is the known anatomical structure of the upper airway. An example of the reconstruction of a representative upper airway from a healthy man is shown in Fig. 3.

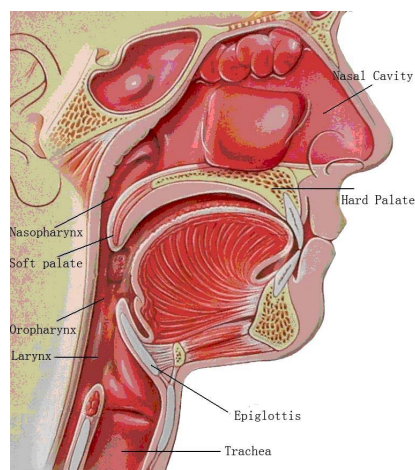


Fig. 2. A sketch showing the known anatomy of the upper airway

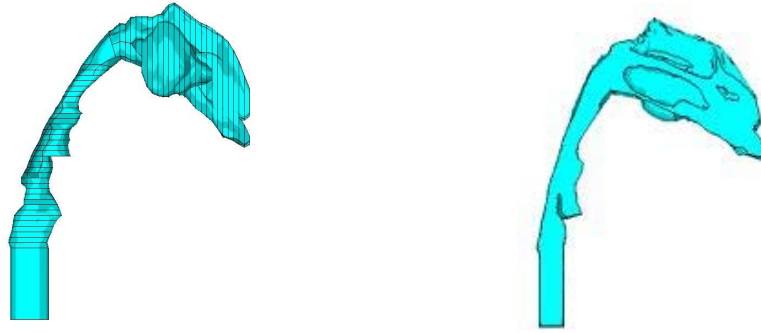


Fig. 3. 3d model of the upper airway (the right figure is the sectional view)

2.2 Numerical methods

The governing equations that are the conservation of mass (continuity) and momentum (Navier-Stokes) are given as follows:

$$\frac{\partial u_i}{\partial x_i} = 0 \tag{1}$$

$$\frac{\partial u_i}{\partial t} + u_j \frac{\partial u_j}{\partial x_j} = -\frac{\partial p}{\partial x_i} + \frac{1}{Re} \frac{\partial}{\partial x_j} \left(\frac{\partial u_i}{\partial x_j} + \frac{\partial u_j}{\partial x_i} \right) \tag{2}$$

where p is the pressure, Re is the Reynolds number, $u_i = U_i/U_{ir}$, $x_i = X_i/d_{ir}$, $p = P/\rho U_{ir}$, U_i is the velocity vector, U_{ir} is the outlet average velocity, d_{ir} is the nasal diameter, ρ is the aerial density.

The reconstruction model is meshed with the tetrahedron element in which the equations can be solved (Fig. 4). The 1-12 sections correspond with selected CT images in the Fig.1. Then the finite element model has been acquired. The course of respiration should be known to decide the boundary condition before computation. In the airflow field of the upper airway model, a no-slip condition ($V_s=0$) is imposed on the surface of the upper airway walls. The nostrils communicate with the outside directly, the pressure on the entrance surface of the nostril is specified as the standard atmosphere pressure ($P=101325pa$). At the outlet of the vocal cord, the velocity condition can be acquired by processing the data of the tidal volume of normal people. The periodic time of respiration and the trend line of airflow flux which is changing with time are established. The literature states that in normal Chinese people the tidal volume, known as their respiration times in a minute, is about 15~25^[4]. The trend line of air flux is recorded (see Fig. 5). This is the main fact in recording all of the boundary conditions.

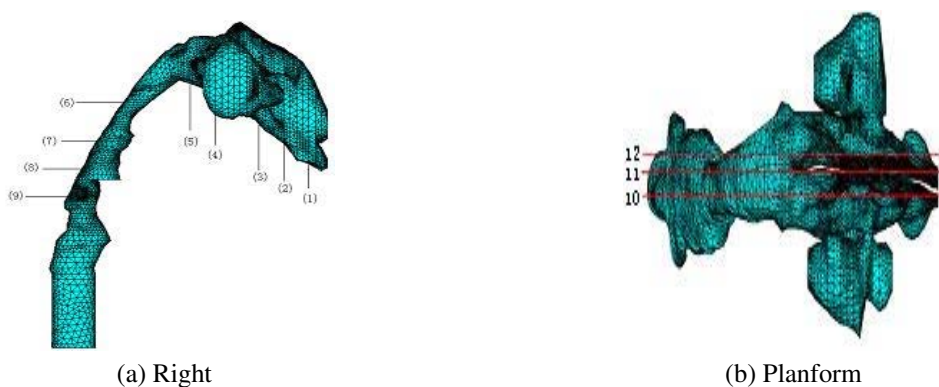


Fig. 4. The three-dimension reconstruction of the upper airway

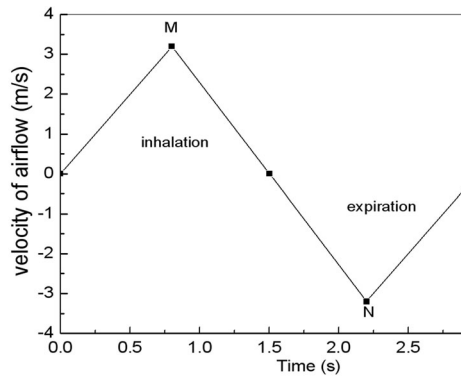


Fig. 5. The airflow velocity in the section of the vocal cord

3 Results

In the current study, the airway in the upper airway is modeled to investigate the effects of flow rate on the flow field and pressure drop. The model in Fig. 4 is a replication of a man’s upper airway cavity. In this model, the sections at the three red lines were selected to display the plot of results at the time of ‘M’ point.

The time of ‘M’ point is the moment at which the air flux in the vocal cord region is at the peak value in an inhalation course. At this moment, the airflow velocities in the region of the nasal vestibule and from the soft palate to epiglottis were higher (Fig. 6). From the pressure distribution (Fig. 7), it can be seen that the air pressure in the region of the nasal vestibule declines sharply, and the pressure in the region of the nasal proper cavity and nasopharynx declines slowly. In the region of the pharyngeal cavities, the pressure distribution is even (Fig. 7). From the figures, it can be seen that the change of the pressure gradient in the pharyngeal cavities was located most of the time near the position from the soft palate to the base of the tongue.

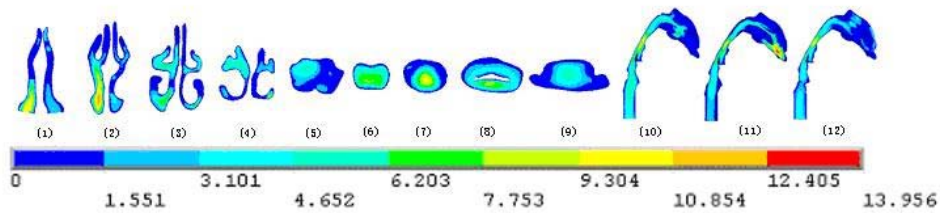


Fig. 6. Velocity distribution at the moment of maximum airflow flux during inspiration, and indices 1-12 refer to sections in fig. 3

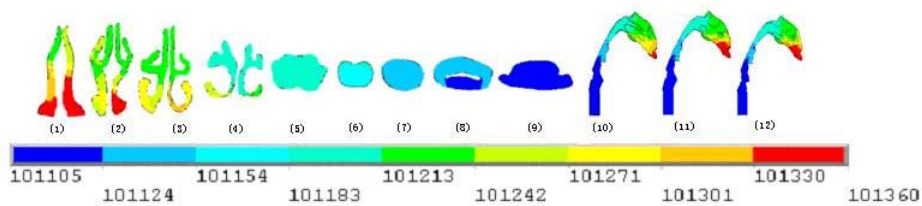


Fig. 7. Pressure distribution at the moment of maximum airflow flux during inspiration, and indices 1-12 refer to sections in fig. 3

4 Discussion

The nasal airway resistance of healthy people is $R_n = 0.126 \sim 0.328$ kPa·s/L^[4] when the highest speed of breathing is V_{max} is equal to 8m/s^[4]. Zhao Ming-hua, using the impulse oscillometry, found that the upper airway impedance of healthy people was $R_a = 0.3086 \pm 0.0839$ kPa·s/L^[11].

The numerical simulations are compared with the data from the literature. The results of ten examples of numerical simulations will satisfy all the requirements shown in Table 1.

Table 2 presents the mean pressure drop ΔP_0 (Pa) between the level section of the hard palate and the base of the tongue at 'M' point and the mean pressure drop ΔP_1 (Pa) between the level section of the hard palate and the vocal cord at 'M' point. Where ΔP_0 was the percentage D (%) of the ΔP_1 ($D = \frac{\Delta P_0}{\Delta P_1} \times 100\%$).

Table 1. The results of the numerical simulation of upper airways in 10 volunteers at 'm' point

Volunteers number	P_{max} (Pa)	P_{min} (Pa)	R_n (kPa s/L)	R_a (kPa s/L)	V_{max} (m/s)
1	101360	101105	0.188	0.272	13.956
2	101353	101092	0.175	0.269	10.575
3	101359	101074	0.193	0.282	13.309
4	101462	101161	0.216	0.324	14.135
5	101360	101077	0.221	0.315	10.687
6	101356	101069	0.184	0.270	12.534
7	101362	101082	0.196	0.284	11.255
8	101357	101077	0.191	0.279	13.078
9	101363	101103	0.203	0.302	12.233
10	101361	101090	0.210	0.308	11.299
$\bar{x} \pm s$	101369.3± 32.70763	101093± 26.76648	0.1977± 0.01462	0.2905± 0.02009	12.3061± 1.31078

Table 2. The results of the numerical simulation of pharyngeal cavities in 10 volunteers at 'm' point

Volunteers number	ΔP_0 (Pa)	ΔP_1 (Pa)	D(%)
1	44.92	59.51	75.48
2	43.96	63.41	69.33
3	42.09	61.30	68.66
4	54.92	70.73	77.65
5	48.82	65.39	74.66
6	54.39	72.08	75.46
7	49.61	68.29	72.65
8	56.39	73.33	76.89
9	47.81	65.27	73.25
10	45.36	63.23	71.74
$\bar{x} \pm s$	48.827±1.57508	66.254±4.68049	73.577±3.02692

5 Conclusions

From the above examples, it can be concluded that the method in this paper is feasible to accurately reconstruct the three-dimensional numerical model of the anatomical upper airway. Compared with the data in the literature, the result obtained from the numerical simulation of the airflow on the model is believable. The characteristic of the method is that the indefinite disturbance factor in the model experiment can be removed and the very difficult phenomenon observed by way of the experiment can be observed. It may be helpful and instructive to reconstruct some similar tissues of the human body.

Based on this study, the air pressure and velocity distributions of healthy people's upper airway obtained by the airflow-field numerical simulation and the statistic of pressure gradient change in the pharyngeal cavity can provide screening of the disease related to the anatomical structure of the upper airway. This study may be useful to forecast and prevent upper airway maladies. In addition, it is also helpful for the quantitative analysis of an operation.

6 Acknowledgments

The authors would like to acknowledge the financial support from the National Natural Science Foundation (No.10472025) and Natural Science Foundation of Liaoning Province (No. 20032109). A special note of thanks is extended to Yanliang Li, Liancheng Zhao and all the doctors of the Department of ENT., Second Affiliated Hospital of Dalian Medical University for their assistance in the design and organization of this research.

References

- [1] F. Alipour, R. Scherer, Knowles. Velocity distributions in Glottal Models. *J. Voice*, 1996, **10**: 50–58.
- [2] T. E. Corcoran, N. Chigier. Characterization of the laryngeal jet using phase doppler interferometry. *J. Aerosol Med*, 2000, **13**: 125–137.
- [3] T. Gemci, T. E. Corcoran, N. Chigier. A numerical and experimental study of spray dynamics in a simple throat model. *Aerosol Sci. Technol*, 2002, **36**: 18–38.
- [4] X. Z. Huang, J. B. Wang. *Practical Otorhinalaryngology*. M. People's Medical Publishing House, 1998.
- [5] M. R. Kaazempur-Mofrad, M. Bathe, H. Karcher, et al. Role of simulation in understanding biological systems. *J. Computers and Structures*, 2003, **81**: 715–726.
- [6] I. M. Katz, T. B. Martonen. Flow patterns in the three-dimensional laryngeal models. *Aerosol Medicine*, 1996, **9**: 501–511.
- [7] S. K. Kim, S. K. Chung. An investigation on airflow in disordered nasal cavity and its corrected models by tomographic PIV. *J. Measurement Science and Technology*, 2004, **15**: 1090–1096.
- [8] C. Kleinstreuer, Z. Zhang. Laminar-to-turbulent fluid-particle flows in a human airway model. *Int. J. Multiphase Flow*, 2003, **29**: 271–289.
- [9] K. W. Stapleton, E. Guentsch, M. K. Hoskinson, et al. On the suitability of k-epsilon modeling for aerosol deposition in the mouth and throat: A comparison with experiment. *J. Aerosol Sci*, 2000, **31**: 739–749.
- [10] R. P. Subramaniam, R. B. Richardson, K. T. Morgan, et al. Computational fluid dynamics simulations of inspiratory airflow in the human nose and nasopharynx. *Inhalation Toxicology*, 1998, **10**: 473–502.
- [11] M. H. Zhao, H. Chen, K. S. Han. A comparison study of impulse oscillometry and polysomnograph in the diagnosis of OSAS. *J. The Journal of Practical Medicine*, 2001, **17**: 693–694.